

# Microtextured CoCrMo alloy for use in metal-on-polyethylene prosthetic joint bearings: Multi-directional wear and corrosion measurements



J. Langhorn<sup>b</sup>, A. Borjali<sup>a</sup>, E. Hippensteel<sup>b</sup>, W. Nelson<sup>b</sup>, B. Raeymaekers<sup>a,\*</sup>

<sup>a</sup> Department of Mechanical Engineering, University of Utah, Salt Lake City, UT, 84112, USA

<sup>b</sup> DePuy Synthes Joint Reconstruction, Warsaw, IN, 46582, USA

## ARTICLE INFO

### Keywords:

Prosthetic hip implant  
Microtexture  
Elastohydrodynamic lubrication  
Polyethylene wear

## ABSTRACT

The longevity of metal-on-polyethylene (MoP) prosthetic hip joint bearings, in which a polished CoCrMo femoral head articulates with a polyethylene liner, may be limited by mechanical instability or inflammation resulting from osteolysis caused by polyethylene wear debris. This study uses laser surface texturing to manufacture a pattern of shallow spherical microtexture features on a polished CoCrMo surface. Gravimetric wear measurements of a highly-crosslinked polyethylene pin articulating with a CoCrMo disc under multi-directional shear demonstrate that polyethylene wear is reduced by more 50% when articulating with a microtextured as opposed to a polished CoCrMo disc. Electrochemical measurements also show that laser texturing does not negatively affect the corrosion potential of CoCrMo.

## 1. Introduction

Total hip replacement (THR) is a surgical procedure in which a patient's natural hip joint is replaced with a prosthetic hip implant. Approximately 300,000 THR surgeries are performed annually in the United States (2015 data [1]), and this number is projected to grow due to the increased prevalence of degenerative joint diseases such as arthritis, and the success of prosthetic hip implants in improving a patient's quality of life [2].

A prosthetic hip implant typically comprises a femoral head component that is attached to a metal alloy stem fixed in the patient's femur, and articulates with an acetabular liner that is secured in an acetabular shell anchored in the pelvis, thus replacing the natural hip joint function. Several material combinations are currently used in prosthetic hip implant bearings, including metal-on-polyethylene (MoP), ceramic-on-polyethylene (CoP), and ceramic-on-ceramic (CoC). In 2012, 56% of all prosthetic hip implants consisted of MoP and 35% of CoP bearings [3]. This work specifically focuses on MoP prosthetic hip implant bearings.

Revision THR surgery, in which a prosthetic hip implant is replaced with a new one, accounts for approximately 10% of all THR surgeries, has a higher number of complications for the patient than primary THR surgery, and is costly for the healthcare system [4]. Therefore, reducing the number of revision surgeries is of critical importance. The most common causes of revision surgery are instability and dislocation of the prosthetic implant (22.5%), mechanical loosening (19.7%), and

infection (14.8%) [4]. It is well-documented that periprosthetic osteolysis attributed to polyethylene wear debris, among other things, can play a crucial role in each of these failure modes, e.g. Refs. [5–9]. Hence, polyethylene wear remains an important problem that must be addressed to further improve the longevity of MoP prosthetic hip implants.

Many researchers have attempted to increase the longevity of MoP prosthetic hip implants by improving the mechanical properties and wear resistance of the polyethylene acetabular liner or, alternatively, by changing the design of the prosthetic hip implant components. For example, highly cross-linking ultra-high molecular weight polyethylene (UHMWPE), and subsequently blending or infusing it with anti-oxidant materials such as vitamin E, has significantly reduced polyethylene wear and successfully increased the longevity of MoP prosthetic implants, e.g. Refs. [10–14]. Using new materials such as titanium and zirconia [15–18], and manufacturing ultra-smooth bearing surfaces have also been implemented successfully, as indicated by the increased interest in CoP and CoC prosthetic hip implants [3,19–21].

This study uses laser surface texturing to manufacture a patterned microtexture on the CoCrMo metal alloy and reduce polyethylene wear in MoP bearing couples for possible implementation in prosthetic hip implants. The patterned microtexture comprises an array of shallow, concave, spherical microtexture features on a polished CoCrMo surface and does not alter the surface roughness of the area in between the microtexture features. The shallow microtexture features are specifically designed to form microhydrodynamic bearings that increase the

\* Corresponding author.

E-mail address: [bart.raeymaekers@utah.edu](mailto:bart.raeymaekers@utah.edu) (B. Raeymaekers).

lubricant film thickness and reduce contact between the CoCrMo and polyethylene bearing surfaces and, thus, reduce polyethylene wear. This approach contrasts with previous studies that involved microtextured bearing surfaces for prosthetic hip implants, which attempted to use the microtexture features as microscale lubricant reservoirs and/or accumulation areas (“traps”) for wear particles. Sawano et al. [22], and Cho et al. [23] performed pin-on-disc (PoD) wear experiments using a polyethylene pin articulating with a CoCrMo disc with various microtexture designs, and they documented that the friction coefficient and polyethylene wear decrease when articulating with a microtextured compared to a non-textured CoCrMo disc. Ito et al. [24] used a microtextured CoCrMo femoral head in a hip simulator, and also reported reduced wear compared to using non-textured CoCrMo specimens. Furthermore, Chyr et al. [25] used a cylindrical surrogate CoCrMo femoral head with a patterned microtexture specifically designed to create microhydrodynamic bearings, which articulated with a conformal cylindrical UHMWPE liner. They documented that the friction coefficient between the UHMWPE and the microtextured CoCrMo specimens is lower than that with the non-textured CoCrMo specimens, for a range of operating conditions. However, no wear measurements were performed. Borjali et al. [26] recently demonstrated significantly reduced wear of UHMWPE, highly-crosslinked polyethylene (HXPE), and vitamin E-infused highly-crosslinked polyethylene (VEXPE) pins articulating with a microtextured CoCrMo surface specifically designed to create microhydrodynamic bearings. However, only uni-directional shear between the polyethylene pins and the CoCrMo surface was evaluated, whereas multidirectional shear is well-known to increase polyethylene wear [27]. In addition, none of the works documented in the literature have evaluated the effect of laser surface texturing on corrosion resistance of the CoCrMo alloy.

The objective of this study was to experimentally quantify wear of HXPE pins articulating with microtextured and non-textured CoCrMo discs, respectively, under multi-directional shear. Different microtexture designs, selected based on simulations using an elastohydrodynamic lubrication model, were evaluated to determine the effect of microtexture design parameters on HXPE wear. The effect of laser surface texturing on the corrosion resistance of CoCrMo alloy surfaces was also experimentally measured.

## 2. Materials and methods

### 2.1. Lubrication simulations

A soft elastohydrodynamic lubrication (EHL) model, identical to the one used in our previous work [28], was implemented to simulate the pressure, load-carrying capacity, and lubricant film thickness in the interface between the polyethylene pin and the microtextured CoCrMo disc as a function of the operating conditions and microtexture design parameters. The soft EHL model was used to quantify the effect of microtexture geometry on lubricant film thickness, and then informed the choice of microtexture designs used in the wear experiments.

This steady-state model accounted for axial loading (load-carrying capacity  $W = 0.50$  MPa) of the polyethylene pin and uni-directional sliding with respect to the CoCrMo disc ( $U = 0.10$  m/s). Only spherical microtexture features were considered because a hip implant is subject to 3D kinematics, thereby requiring axisymmetric texture features for identical performance in all directions. Fig. 1 A displays a top view of a section of the microtextured CoCrMo surface ( $E_{CoCrMo} = 230$  GPa,  $\nu_{CoCrMo} = 0.3$  [29]) showing an  $N$ -by- $N$  array of spherical microtexture features of radius  $r_p$  and depth  $h_p$  ( $N = 8$  in this work). Fig. 1 B depicts a cross-sectional view of the interface between the microtextured CoCrMo surface and the smooth, deformable polyethylene surface ( $E_{poly} = 1$  GPa,  $\nu_{poly} = 0.4$  [30]), representing the pin, and separated by an incompressible lubricant of minimum thickness  $c$ .

A constant dynamic viscosity  $\mu = 1.0$  Pa s was used in the numerical model to ensure stability of the numerical simulation, which required

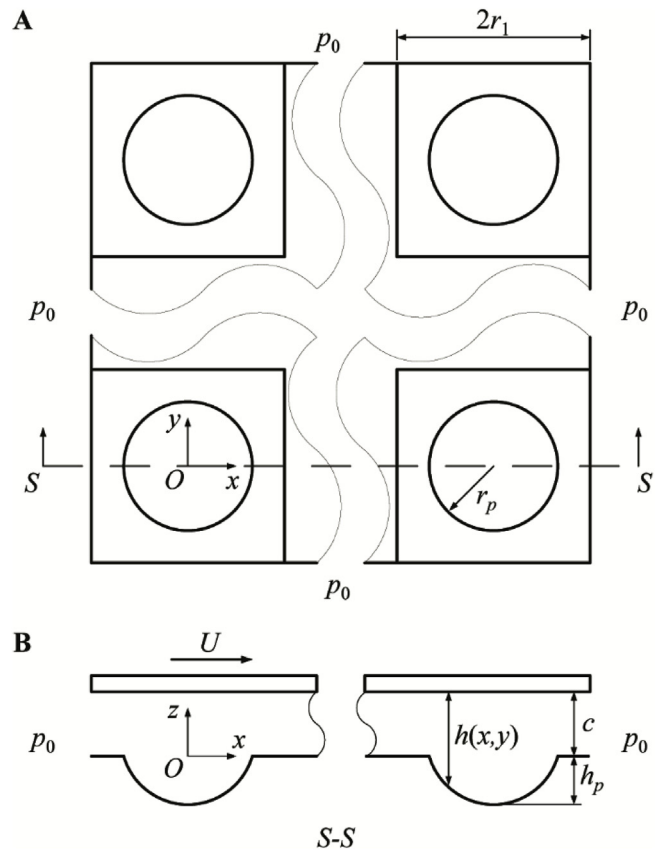


Fig. 1. (A) top view of the rigid, microtextured CoCrMo surface and (B) cross-sectional view of the microtextured CoCrMo surface and deformable polyethylene surface.

simultaneous solution of the pressure in the lubricant film, and the resulting elastic deformation of the polyethylene, while balancing the external bearing load. However, the viscosity is believed to have little influence on relative performance of different microtexture designs [30]. The load-carrying capacity of the lubricant film per unit area,  $W$ , was computed as

$$W = \frac{1}{A} \iint_{\Omega} p(x, y) dx dy \quad (1)$$

The steady-state incompressible Reynolds equation relates the local pressure  $p(x, y)$  to lubricant film thickness  $h(x, y)$  for a set of operating parameters ( $U, \mu, W$ ) and for a specific microtexture design ( $\epsilon = h_p/2r_p$  and  $S_p = \pi(r_p/2r_1)^2$ ) [31].

$$\frac{\partial}{\partial x} \left( h^3 \frac{\partial p}{\partial x} \right) + \frac{\partial}{\partial y} \left( h^3 \frac{\partial p}{\partial y} \right) = 6\mu U \frac{\partial h}{\partial x} \quad (2)$$

Here,

$$h(x, y) = \begin{cases} c + d(x, y), & \text{if } x^2 + y^2 > r_p^2 \\ c + \sqrt{\frac{1}{4} \left( h_p + \frac{r_p^2}{h_p} \right)^2 - (x^2 + y^2)} + \frac{1}{2} \left( h_p - \frac{r_p^2}{h_p} \right) + d(x, y), & \text{if } x^2 + y^2 \leq r_p^2 \end{cases}$$

$d(x, y)$  is the polyethylene deformation, computed from the local pressure  $p(x', y')$  of all  $(x', y')$  in the solution domain  $\Omega$ .

$$d(x, y) = \frac{1 - \nu_{poly}^2}{\pi E_{poly}} \iint_{\Omega} \frac{p(x', y')}{\sqrt{(x' - x)^2 + (y' - y)^2}} dx' dy' \quad (3)$$

Ambient pressure,  $p_0$ , was imposed on all four edges of the solution domain. The Reynolds cavitation boundary condition ensured that the pressure cannot drop below the ambient pressure in the cavitation region, and the pressure gradient is zero at the boundary of the cavitation

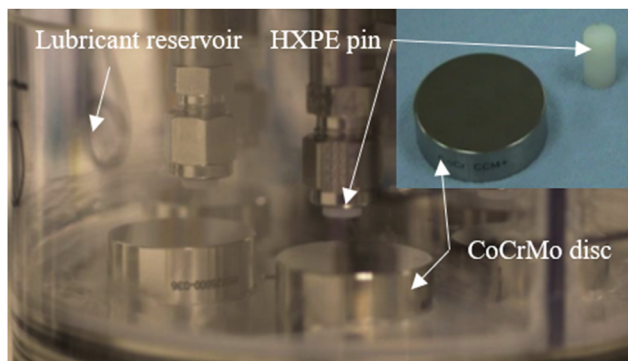


Fig. 2. Experimental setup showing CoCrMo disc and HXPE pin specimens.

region [32]. A finite difference discretization on a uniform grid with 129 by 129 nodes per unit cell together with the Effective Influence Newton (EIN) method [33] and the Multi-Level Multi-Integration (MLMI) method [34] was used to simultaneously solve Eqs. (1)–(3).

### 2.2. Wear experiments

Gravimetric wear measurements were performed using an AMTI OrthoPOD machine using an HXPE (GUR 1020, extruded, annealed, gamma irradiated with 5.0 MRad) pin with a flat, fly cut machined surface articulating with a CoCrMo alloy disc surface. Fig. 2 shows a picture of the experimental setup.

The articulating surface of the pin was oriented at  $90^\circ \pm 2^\circ$  with respect to the disc surface and moved in a  $10 \times 20$  mm square kinematic cycle at a frequency of 1.6 Hz, producing multi-directional shear with respect to the disc. A Paul loading cycle [35] was applied, with a peak load of 330 N, resulting in a 4.65 MPa peak contact pressure between pin and disc. Peak loads of the Paul cycle (“heel strike” and “toe off”) were designed to occur at two corners of the kinematic cycle to maximize wear at points of highest cross-shear, as would occur in the walking gait cycle of the human hip. Fig. 3 visualizes the kinematic cycle of the pin with respect to the disc in an x-y plane, with the external loading of the pin superimposed (z-axis).

The pins and discs were submerged in bovine serum maintained at 37 °C (HyClone Laboratories Inc., Logan, UT) and diluted with reverse osmosis water to reach a protein concentration of 64.8 mg/mL. It is noted that the protein concentration used in this study was higher than commonly used in PoD experiments. This helped observe increases in measured wear rates of highly-crosslinked polyethylene, when articulated with different counterface surfaces, and discern otherwise small differences of polyethylene wear. 0.2% sodium azide was added to inhibit bacterial growth and 20 mM ethylenediaminetetraacetic acid (EDTA) to stabilize calcium phosphate.

Twelve HXPE pins (9.5 mm diameter, 18 mm length) were manufactured for this study. The surface topography of the flat articulating end of the pin was similar to that of commercially available

Table 1  
Overview of CoCrMo disc specimens and microtexture parameters.

Disc ID	Microtexture parameters				
	Depth, $h_p$ [μm]	Diameter $d_p$ [μm]	Pitch $r_1$ [μm]	Aspect ratio $\epsilon = h_p/d_p$	Density $S_p = \pi d_p^2/4r_1^2$
1a	2.00	100	296	0.020	0.10
1b	2.00	100	296	0.020	0.10
2a	2.00	100	198	0.020	0.20
2b	2.00	100	198	0.020	0.20
3	1.00	100	296	0.010	0.10
4	0.50	100	396	0.005	0.05
Control ( $N = 3$ )	0.00	0	0	0.000	0.00

polyethylene acetabular liners with average surface roughness  $R_a < 1.5 \mu\text{m}$ . White light interferometry was used to inspect the surface roughness of the polyethylene pins. Nine pins were used in PoD wear experiments and three pins were used as soak compensation specimens for the gravimetric wear measurements. Nine CoCrMo discs (38.1 mm diameter, 12.5 mm thick, ASTM F1537 [36]) were polished to a surface finish similar to that of commercially available CoCrMo femoral heads with  $R_a < 50 \text{ nm}$ . Laser surface texturing [31] with a femtosecond laser ablation process was used to manufacture the microtexture on the surface of six CoCrMo discs, according to the specifications shown in Table 1. The different microtexture designs were selected based on the numerical simulation results, to increase the lubricant film thickness between the CoCrMo and polyethylene bearing surfaces. White light interferometry was employed to determine that no “ridges” of re-deposited material existed around the contour of the microtexture features after laser surface texturing. Three discs remained non-textured and were used as control specimens. Note that the microtexture geometry on disc 1a and 1b, and 2a and 2b, respectively, are identical.

Wear experiments were conducted for a total of 1.98 million cycles. At each 0.33 million cycle interval the bovine serum was replaced and the polyethylene pins were cleaned, dried, and measured gravimetrically using an XP205 balance (Mettler Toledo, Columbus OH) per ISO 14242-2 [37]. The HXPE wear rate was calculated using a least-squares linear regression excluding the 0 cycle, 0 wear data point.

### 2.3. Corrosion experiments

Electrochemical Impedance Spectroscopy (EIS) and Cyclic Potentiodynamic Polarization (CPP), according to ASTM G61 [38], were used to characterize corrosion of laser-textured CoCrMo discs in phosphate-buffered saline electrolyte (NERL Blood Bank Saline, Thermo Scientific) with an Ametek Model K0235 flat cell. This cell used an ALS RE-1C Ag/AgCl reference electrode with saturated KCl and a Bio-Logic A-702439 platinum mesh counter electrode. The cell was connected to a Bio-logic SP-200 Potentiostat (S/N 0407). Microtextured discs, previously used in the PoD wear test, were compared to a non-textured control. All electrochemical tests covered a  $1 \text{ cm}^2$  area of each disc on all microtextured discs (discs 1–4) and the non-textured discs, respectively. Prior to the experiment, the discs were cleaned in an ultrasonic cleaner (Branson 2510) for 15 min in 1% alconox detergent (Alconox Inc.) and then rinsed with reverse osmosis water and sonicated for 10 min in denatured ethanol. The discs were dried in ambient air for 20 min. Open Circuit Potential (OCP) measurements were performed to quantify the variation of the electrochemical processes occurring on the surface of the discs as a function of time, which may indicate corrosion. Electrochemical Impedance Spectroscopy (EIS) was performed to quantify the polarization resistance ( $R_p$ ) of the discs, which directly correlates to the corrosion rate. During this experiment, a 5–10 mV AC excitation voltage was applied to a disc and the impedance of the metal-

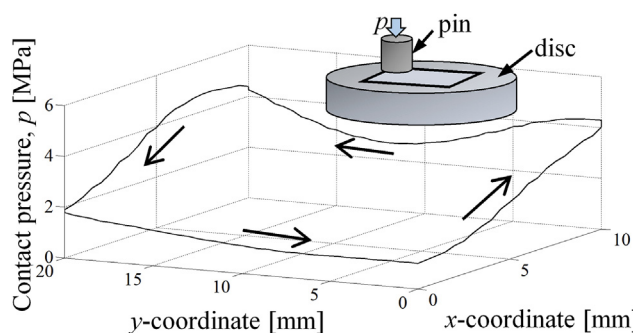


Fig. 3. Contact pressure and kinematic cycle used in the PoD wear experiment.

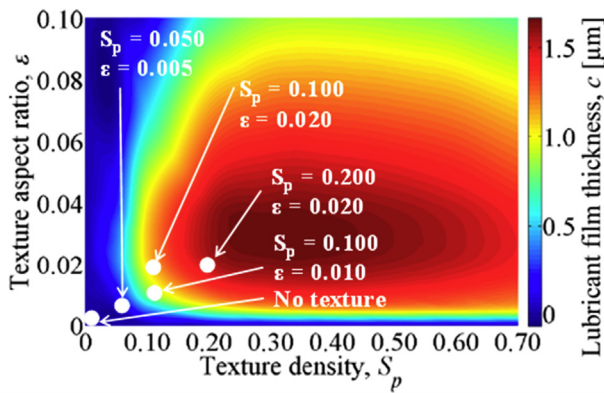


Fig. 4. Elastohydrodynamic lubrication simulation results, showing minimum lubricant film thickness as a function of texture aspect ratio and texture density, also identifying different microtexture designs for wear experiments.

solution interface was measured.  $R_p$  was derived from the impedance versus frequency plot and subtracting the impedance at the high-frequency limit ( $10^6$  Hz) from the impedance at the low-frequency limit ( $10^{-1}$  Hz). Cyclic Potentiodynamic Polarization (CPP) measurements were performed to determine the relative susceptibility of the discs to (localized) corrosion. The potential-current relationship was measured, allowing a Tafel fit to be made, and estimating the corrosion rate of the disc at the OCP, which cannot be measured directly [39]. Note that EIS and CPP measurements were performed under “steady-state” conditions, i.e., when the concentration of products and reactants at the corroding surface and the rate of the corrosion reaction are constant. In this work, the disc was considered to be in “steady state” if the OCP did not change more than 10 mV/h. It is also noted that evaluating  $N = 1$  for each microtextured disc type was an effective screening test for localized corrosion rather than a method to quantify corrosion rates for these surface textures.

### 3. Results and discussion

#### 3.1. Simulation results

Fig. 4 depicts the minimum lubricant film thickness for constant operating conditions ( $\mu = 1.0$  Pa s,  $U = 0.10$  m/s,  $W = 0.50$  MPa), as a function of the texture aspect ratio  $\epsilon$  and the texture density  $S_p$ , simulated using the elastohydrodynamic (EHL) lubrication model. The minimum lubricant film thickness  $c$  between the CoCrMo and polyethylene bearing surfaces is largest for  $0.20 \leq S_p \leq 0.40$  and  $0.01 \leq \epsilon \leq 0.04$ . This is in agreement with EHL simulations of microtextured bearings performed by others, including Gao et al. [40]. Fig. 4 also indicates four different microtexture designs (white dots) that were selected for evaluation in the wear experiments, as listed in Table 1.

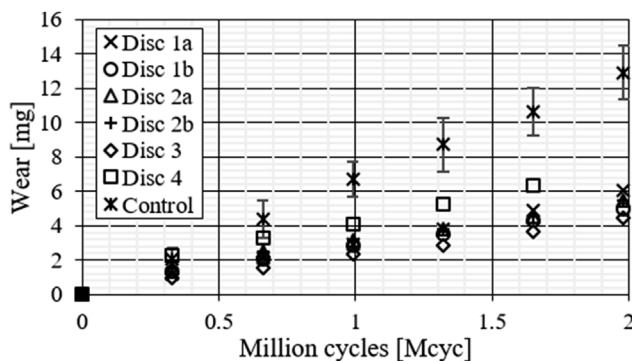


Fig. 5. Wear as a function of cycles in the pin-on-disc wear experiment, for all textured and non-textured discs articulating with an HXPE pin.

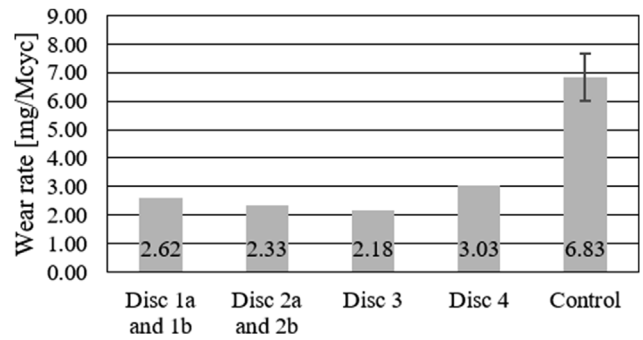


Fig. 6. Average wear rate for all HXPE pins articulating with textured and non-textured CoCrMo discs under multi-directional shear (error bars represent  $\pm 80\%$  CI).

#### 3.2. Wear experiments

Fig. 5 shows cumulative gravimetric polyethylene wear as a function of the number of kinematic cycles, for HXPE pins articulating with each of the different CoCrMo discs, selected from the simulation results (indicated in Fig. 4). The error bars of the data points of the control specimen ( $N = 3$ ) represent the 80% confidence interval. Wear of the HXPE pin increases as a function of the number of cycles, i.e., the sliding distance. No difference in polyethylene wear was measured between the discs with different microtexture designs. However, less polyethylene wear was measured for all pins articulating with a microtextured compared to a non-textured disc. It is noted that the microtexture design of disc 4 has the shallowest microtexture features ( $\epsilon = 0.005$ ) and the lowest texture density ( $S_p = 0.05$ ) of all microtexture designs evaluated in this work. White light interferometry of the surface of the polyethylene pins that articulated with the microtextured discs showed a smaller increase in average surface roughness after the wear test, than the surface of the pins that articulated with the non-textured discs. This is similar to our results documented for uni-directional sliding [26], and indicates that the reduced polyethylene wear is due to the formation of a lubricant film instead of simply a reduction in contact area as a result of the microtexture features. In fact, the microtexture could even increase polyethylene wear if it fails to create a lubricant film, because a reduced contact area causes increased contact stress in the polyethylene for the same bearing load-carrying capacity, which may cause fatigue wear. Comparing results of Fig. 5 to the steady-state elastohydrodynamic lubrication simulation results of Fig. 4, it is apparent that a surface microtexture with  $\epsilon = 0.005$  and  $S_p = 0.05$  did not result in a significant increase of the lubricant film thickness between the bearing surfaces, in contrast with the other microtexture designs used in this study. As a result, contact between the HXPE pin and disc 4 is greater than with the other discs, potentially increasing wear.

Fig. 6 shows the average wear rate computed over 1.98 million cycles for all HXPE pins articulating with textured and non-textured CoCrMo discs. For the control specimens ( $N = 3$ ), the average value

Table 2

Corrosion potential, corrosion current, and corrosion rates determined from Tafel fits. The number in parentheses next to the control specimens is the standard deviation ( $N = 4$ ). The  $R_p$  value was determined via EIS.

Disc ID	$E_{corr}$ (mV)	$I_{corr}$ (nA)	Corrosion Rate ( $\mu\text{g}/\text{y}$ )	Polarization Resistance $\text{M}\Omega\text{cm}^2$
Disc 1a, 1 b	-165	0.2	1.2	1.80
Disc 2a, 2 b	-93	0.06	0.48	2.10
Disc 3	-145	0.08	0.63	1.95
Disc 4	-79	0.2	1.7	1.89
Control ( $N = 4$ )	-136 (9.7)	1.49 (0.6)	11.6 (4.6)	2.00 (0.19)

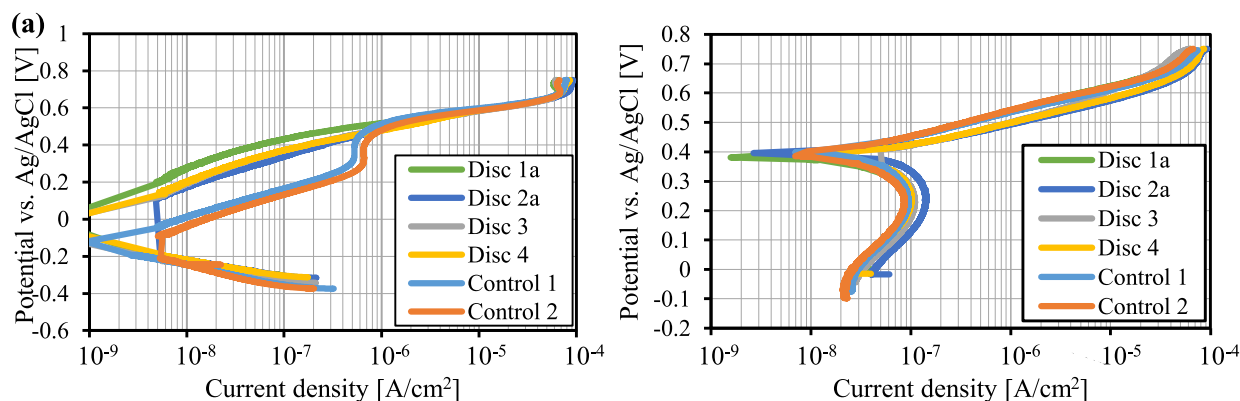


Fig. 7. CPP measurements of textured and non-textured discs, showing (a) the forward scan and (b) the return scan, separated from each other for clarity.

was reported, and the error bars indicate the 80% confidence interval. All microtexture designs reduced polyethylene wear by more than 50%, when comparing the average wear rate of HXPE that articulated with the different microtextured discs and the traditional polished, non-textured CoCrMo disc. This result qualitatively agrees with earlier studies that have documented a significant reduction of polyethylene wear when articulating with textured as opposed to non-textured CoCrMo surfaces [22–25]. However, based on the geometry of the texture features reported in these previous publications, they did not create microhydrodynamic bearings (aspect ratio too large), but served as lubrication reservoirs and wear particle traps. In this work, examination of the shallow texture features did not reveal wear particles being accumulated, likely because the shallow microtexture features are not deep enough to house them. Additionally, both pins and discs were cleaned every 0.33 million cycles to ensure that the polyethylene wear reduction attributed to the microtexture is entirely due to the increase in lubricant film thickness between the bearings surfaces created by the microhydrodynamic bearings. The wear results documented in this work also corroborate those of our earlier work [26], which showed gravimetric wear measurements under uni-directional shear and constant loading, performed on a PoD apparatus developed at the University of Utah as opposed to the commercially available AMTI OrthoPOD used in this work. Furthermore, the wear results show that the elastohydrodynamic lubrication model can be used to predict microtexture geometries that will result in a reduction of polyethylene wear. However, the gravimetric wear results did not allow distinguishing significantly different polyethylene wear between different microtexture designs.

### 3.3. Corrosion experiments

The OCP measurements of all (textured and non-textured) CoCrMo discs reached steady-state after 3 h, indicating that the electrochemical processes occurring on the surface of the discs were stable as a function of time at the beginning of the test. Table 2 shows that the polarization resistance  $R_p$  for each of the textured and non-textured CoCrMo discs is on the order of  $10^6$ – $10^7 \Omega\text{cm}^2$ , which is consistent with previously published EIS data for CoCrMo in joint fluid [41]. A single time constant was observed in the measurements, which indicates an intact and nonporous oxide layer on the surface of the CoCrMo disc.

Furthermore, the CPP measurements were used to determine Tafel plots from which the corrosion potential and current,  $E_{corr}$  and  $I_{corr}$ , are derived, and the corrosion rate at the OCP estimated. Fig. 7(a) and (b) show representative forward and reverse CPP curves, respectively, measured on non-textured and several microtextured CoCrMo disc surfaces. The CPP results demonstrate that the surface of both textured and non-textured discs is passive, i.e., the current density is less than  $10 \mu\text{A}$  for a wide range of potentials, and no significant corrosion

occurs. Furthermore, no hysteresis is observed in the return scans, which suggests that none of the discs were vulnerable to localized corrosion. Thus, the results of the CPP and EIS measurements do not indicate that the laser textured CoCrMo material is more vulnerable to corrosion than a non-textured surface. In the forward scans (Fig. 7 (a)), it is noted there is a discontinuous portion of the CPP curve, from  $-200 \text{ mV}$  to  $+300 \text{ mV}$  on some discs. In this range, the current generated is less than  $5 \text{ nA}$ , which was not measurable by the potentiostat equipment. Repeat measurements with a potentiostat capable of current measurements between  $10^{-8}$  to  $10^{-12} \text{ A}$  could reveal the corrosion behavior in this range.

## 4. Conclusions

A patterned microtexture on a CoCrMo disc, specifically designed to create microhydrodynamic bearings reduced polyethylene wear under multi-directional shear conditions by more than 50% compared to non-textured polished discs. The microhydrodynamic bearings increase the lubricant film thickness between the CoCrMo and polyethylene bearing surfaces, thereby reducing contact and wear. Additionally, the corrosion measurements indicated that the laser surface textured CoCrMo material does not suffer from increased vulnerability to corrosion compared to the non-textured CoCrMo material.

## Acknowledgments

A.B. and B.R. acknowledge support from the National Institutes of Health, National Institute of Arthritis and Musculoskeletal and Skin Diseases under grant 1R03AR066826-01A1.

## References

- [1] Total Hip Replacement - OrthoInfo - AAOS. Website Am Acad Orthop Surg August 2015 n.d. <https://orthoinfo.aaos.org/en/treatment/total-hip-replacement> (accessed December 29, 2017).
- [2] Maradit Kremers H, Larson DR, Crowson CS, Kremers WK, Washington RE, Steiner CA, et al. Prevalence of total hip and knee replacement in the United States. *J Bone Jt Surg Am Vol* 2015;97:1386–97. <http://dx.doi.org/10.2106/JBJS.N.01141>.
- [3] Lehl MS, Bozic KJ. Trends in total hip arthroplasty implant utilization in the United States. *J Arthroplasty* 2014;29:1915–8. <http://dx.doi.org/10.1016/j.arth.2014.05.017>.
- [4] Bozic KJ, Kurtz SM, Lau E, Ong K, Vail TP, Berry DJ. The epidemiology of revision total hip arthroplasty in the United States. *J Bone Jt Surg Am Vol* 2009;91:128–33. <http://dx.doi.org/10.2106/JBJS.H.00155>.
- [5] Dumbleton JH, Manley MT, Edidin AA. A literature review of the association between wear rate and osteolysis in total hip arthroplasty. *J Arthroplasty* 2002;17:649–61.
- [6] Badarudeen S, Shu AC, Ong KL, Baykal D, Lau E, Malkani AL. Complications after revision total hip arthroplasty in the medicare population. *J Arthroplasty* 2017;32:1954–8. <http://dx.doi.org/10.1016/j.arth.2017.01.037>.
- [7] Hallab NJ, Jacobs JJ. Chemokines associated with pathologic responses to orthopedic implant debris. *Front Endocrinol* 2017;8:5. <http://dx.doi.org/10.3389/fendo>.

- 2017.00005.
- [8] Sadoghi P, Liebensteiner M, Agreiter M, Leithner A, Böhler N, Labek G. Revision surgery after total joint arthroplasty: a complication-based analysis using worldwide arthroplasty registers. *J Arthroplasty* 2013;28:1329–32. <http://dx.doi.org/10.1016/J.ARTH.2013.01.012>.
- [9] Ormsby RT, Cantley M, Kogawa M, Solomon LB, Haynes DR, Findlay DM, et al. Evidence that osteocyte perilacunar remodelling contributes to polyethylene wear particle induced osteolysis. *Acta Biomater* 2016;33:242–51. <http://dx.doi.org/10.1016/J.ACTBIO.2016.01.016>.
- [10] Kurtz SM, Gawel HA, Patel JD. History and systematic review of wear and osteolysis outcomes for first-generation highly crosslinked polyethylene. *Clin Orthop Relat Res* 2011;469:2262–77. <http://dx.doi.org/10.1007/s11999-011-1872-4>.
- [11] Kurtz SM, Patel JD. The clinical performance of highly cross-linked UHMWPE in hip replacements. *UHMWPE biomater. Handb. Elsevier*; 2016. p. 57–71. <http://dx.doi.org/10.1016/B978-0-323-35401-1.00006-5>.
- [12] Devane PA, Horne JG, Ashmore A, Mutimer J, Kim W, Stanley J. Highly cross-linked polyethylene reduces wear and revision rates in total hip arthroplasty. *J Bone Jt Surg* 2017;99:1703–14. <http://dx.doi.org/10.2106/JBJS.16.00878>.
- [13] Hanna SA, Somerville L, McCalden RW, Naudie DD, MacDonald SJ. Highly cross-linked polyethylene decreases the rate of revision of total hip arthroplasty compared with conventional polyethylene at 13 years' follow-up. *Bone Joint Lett J* 2016;98:B:28–32. <http://dx.doi.org/10.1302/0301-620X.98B1.36527>.
- [14] Tsukamoto M, Mori T, Ohnishi H, Uchida S, Sakai A. Highly cross-linked polyethylene reduces osteolysis incidence and wear-related reoperation rate in cementless total hip arthroplasty compared with conventional polyethylene at a mean 12-year follow-up. *J Arthroplasty* 2017;32:3771–6. <http://dx.doi.org/10.1016/j.arth.2017.06.047>.
- [15] Yang Y. Deposition of highly adhesive ZrO<sub>2</sub> coating on Ti and CoCrMo implant materials using plasma spraying. *Biomaterials* 2003;24:619–27. [http://dx.doi.org/10.1016/S0142-9612\(02\)00376-9](http://dx.doi.org/10.1016/S0142-9612(02)00376-9).
- [16] Agarwal A, Dahotre NB. Mechanical properties of laser-deposited composite boride coating using nanoindentation. *Metall Mater Trans* 2000;31:401–8. <http://dx.doi.org/10.1007/s11661-000-0277-x>.
- [17] Aherwar A, Patnaik A, Bahraminasab M, Singh A. Preliminary evaluations on development of new materials for hip joint femoral head. *Proc Inst Mech Eng Part L J Mater Des Appl* 2017. <http://dx.doi.org/10.1177/1464420717714495>. 1464420717714499.
- [18] Affatato S, Ruggiero A, Merola M. Advanced biomaterials in hip joint arthroplasty. A review on polymer and ceramics composites as alternative bearings. *Compos B Eng* 2015(83):276–83. <http://dx.doi.org/10.1016/J.COMPOSITESB.2015.07.019>.
- [19] Sychterz CJ, Engh CA, Young AM, Hopper RH, Engh CA. Comparison of in vivo wear between polyethylene liners articulating with ceramic and cobalt-chrome femoral heads. *J Bone Joint Surg Br* 2000;82:948–51.
- [20] Rahaman MN, Yao A, Bal BS, Garino JP, Ries MD. Ceramics for prosthetic hip and knee joint replacement. *J Am Ceram Soc* 2007;90:1965–88. <http://dx.doi.org/10.1111/J.1551-2916.2007.01725.X>.
- [21] Atray A, Wolfstadt JI, Hussain N, Khoshbin A, Ward S, Shahid M, et al. The ideal total hip replacement bearing surface in the young patient: a prospective randomized trial comparing alumina ceramic-on-ceramic with ceramic-on-conventional polyethylene: 15-year follow-up. *J Arthroplasty* 2017. <http://dx.doi.org/10.1016/J.ARTH.2017.11.066>.
- [22] Sawano H, Warisawa S, Ishihara S. Study on long life of artificial joints by investigating optimal sliding surface geometry for improvement in wear resistance. *Precis Eng* 2009;33:492–8. <http://dx.doi.org/10.1016/J.PRECISIONENG.2009.01.005>.
- [23] Cho M, Choi H-J. Optimization of surface texturing for contact between steel and ultrahigh molecular weight polyethylene under boundary lubrication. *Tribol Lett* 2014;56:409–22. <http://dx.doi.org/10.1007/s11249-014-0418-9>.
- [24] Ito H, Kaneda K, Yuhta T, Nishimura I, Yasuda K, Matsuno T. Reduction of polyethylene wear by concave dimples on the frictional surface in artificial hip joints. *J Arthroplasty* 2000;15:332–8. [http://dx.doi.org/10.1016/S0883-5403\(00\)90670-3](http://dx.doi.org/10.1016/S0883-5403(00)90670-3).
- [25] Chyr A, Qiu M, Speltz JW, Jacobsen RL, Sanders AP, Raeymaekers B. A patterned microtexture to reduce friction and increase longevity of prosthetic hip joints. *Wear* 2014;315:51–7. <http://dx.doi.org/10.1016/j.wear.2014.04.001>.
- [26] Borjali A, Langhorn J, Monson K, Raeymaekers B. Using a patterned microtexture to reduce polyethylene wear in metal-on-polyethylene prosthetic bearing couples. *Wear* 2017;392–393:77–83. <http://dx.doi.org/10.1016/J.WEAR.2017.09.014>.
- [27] Petersen D, Link R, Wang A, Polineni V, Essner A, Sokol M, et al. The significance of nonlinear motion in the wear screening of orthopaedic implant materials. *J Test Eval* 1997;25:239. <http://dx.doi.org/10.1520/JTE11485J>.
- [28] Qiu M, Chyr A, Sanders AP, Raeymaekers B. Designing prosthetic knee joints with bio-inspired bearing surfaces. *Tribol Int* 2014;77:106–10. <http://dx.doi.org/10.1016/J.TRIBOINT.2014.04.025>.
- [29] Mattei L, Di Puccio F, Piccigallo B, Ciulli E. Lubrication and wear modelling of artificial hip joints: a review. *Tribol Int* 2011;44:532–49. <http://dx.doi.org/10.1016/J.TRIBOINT.2010.06.010>.
- [30] Shinkarenko A, Kligerman Y, Etsion I. The effect of surface texturing in soft elastohydrodynamic lubrication. *Tribol Int* 2009;42:284–92. <http://dx.doi.org/10.1016/J.TRIBOINT.2008.06.008>.
- [31] Etsion I. State of the art in laser surface texturing. *J Tribol* 2005;127:248. <http://dx.doi.org/10.1115/1.1828070>.
- [32] Pinkus O, Sternlicht B. *Theory of hydrodynamic lubrication*. New York: McGraw-Hill; 1961.
- [33] Jagatia M, Jin ZM. Elastohydrodynamic lubrication analysis of metal-on-metal hip prostheses under steady state entraining motion. *Proc Inst Mech Eng Part H J Eng Med* 2001;215:531–41. <http://dx.doi.org/10.1243/0954411011536136>.
- [34] Brandt A, Lubrecht A. Multilevel matrix multiplication and fast solution of integral equations. *J Comput Phys* 1990;90:348–70. [http://dx.doi.org/10.1016/0021-9991\(90\)90171-V](http://dx.doi.org/10.1016/0021-9991(90)90171-V).
- [35] Paul JP. Forces transmitted by joints in the human body. *Proc Inst Mech Eng Conf Proc* 1966;181:8–15. [http://dx.doi.org/10.1243/PIME\\_CONF\\_1966\\_181\\_201\\_02](http://dx.doi.org/10.1243/PIME_CONF_1966_181_201_02).
- [36] ASTM F1537-11. Standard specification for wrought Cobalt-28Chromium-6Molybdenum alloys for surgical implants (UNS R31537, UNS R31538, and UNS R31539). West Conshohocken, PA: ASTM International; 2011 [www.astm.org](http://www.astm.org).
- [37] ISO 14242-2. Implants for surgery - wear of total hip-joint prostheses - Part 2: Methods of measurement. 2016.
- [38] ASTM G61-86. Standard test method for conducting cyclic potentiodynamic polarization measurements for localized corrosion susceptibility of iron-, nickel-, or cobalt-based alloys. West Conshohocken, PA: ASTM International; 2014 [www.astm.org](http://www.astm.org).
- [39] McCafferty E. *Introduction to corrosion science*. Springer; 2010.
- [40] Gao L, Yang P, Dymond I, Fisher J, Jin Z. Effect of surface texturing on the elastohydrodynamic lubrication analysis of metal-on-metal hip implants. *Tribol Int* 2010;43:1851–60. <http://dx.doi.org/10.1016/j.triboint.2010.02.006>.
- [41] Hodgson AWE, Kurz S, Virtanen S, Fervel V, Olsson C-OA, Mischler S. Passive and transpassive behaviour of CoCrMo in simulated biological solutions. *Electrochim Acta* 2004;49:2167–78. <http://dx.doi.org/10.1016/J.ELECTACTA.2003.12.043>.